Journal of
Photonics for Energy

PhotonicsforEnergy.SPIEDigitalLibrary.org

Efficiency droop behavior improvement through barrier thickness modification for GaN-on-silicon light-emitting diodes

An-Jye Tzou
Bing-Cheng Lin
Chia-Yu Lee
Da-Wei Lin
Yu-Kuang Liao
Zhen-Yu Li
Gou-Chung Chi
Hao-Chung Kuo
Chun-Yen Chang

SPIE.

Downloaded From: http://photonicsforenergy.spiedigitallibrary.org/ on 05/11/2015 Terms of Use: http://spiedl.org/terms

Efficiency droop behavior improvement through barrier thickness modification for GaN-on-silicon light-emitting diodes

An-Jye Tzou,[a,b] Bing-Cheng Lin,[b] Chia-Yu Lee,[b] Da-Wei Lin,[b] Yu-Kuang Liao,[a,b] Zhen-Yu Li,[b,c,*] Gou-Chung Chi,[b] Hao-Chung Kuo,[b,*] and Chun-Yen Chang[a,c]

[a]National Chiao Tung University, Department of Electrophysics, 1001 Ta Hsueh Road, Hsinchu 30010, Taiwan

[b]National Chiao Tung University, Department of Photonics and Institute of Electro-Optical Engineering, 1001 Ta Hsueh Road, Hsinchu 30010, Taiwan

[c]Research Center for Applied Sciences, Academia Sinica, 128 Academia Road, Section 2, Nankang, Taipei 11592, Taiwan

Abstract. Crack-free GaN-based light-emitting diodes (LEDs) were grown on 150-mm-diameter Si substrates by using low-pressure metal-organic chemical vapor deposition. The relationship between the LED devices and the thickness of quantum barriers (QBs) was investigated. The crystal quality and surface cracking of GaN-on-Si were greatly improved by an $Al_xGa_{1-x}N$ buffer layer composed of graded Al. The threading dislocation density of the GaN-on-Si LEDs was reduced to $<7 \times 10^8\ cm^{-2}$, yielding LEDs with high internal quantum efficiency. Simulation results indicated that reducing the QB thickness improved the carrier injection rate and distribution, thereby improving the droop behavior of the LEDs. LEDs featuring 6-nm-thick QBs exhibited the lowest droop behavior. However, the experimental results showed an unanticipated phenomenon, namely that the peak external quantum efficiency (EQE) and light output power (LOP) gradually decreased with a decreasing QB thickness. In other words, the GaN-on-Si LEDs with 8-nm-thick QBs exhibited low droop behavior and yielded a good peak EQE and LOP, achieving a 22.9% efficiency droop and 54.6% EQE. *© 2015 Society of Photo-Optical Instrumentation Engineers (SPIE)* [DOI: 10.1117/1.JPE.5.057604]

Keywords: light-emitting diodes; GaN-on-Si; droop behavior improvement; thin barrier; external quantum efficiency.

Paper 14089SS received Oct. 31, 2014; accepted for publication Feb. 2, 2015; published online Mar. 5, 2015.

1 Introduction

In the last decade, GaN-based light-emitting diodes (LEDs) have been widely used because of their ability to tune wavelengths from ultraviolet to visible light. GaN-based LEDs have been widely applied in solid-state lighting (SSL),[1–4] photovoltaics,[5] and thermoelectric applications.[6,7] For general illumination systems, GaN-based LEDs must overcome numerous challenges, such as a green gap,[8] efficiency droop behavior,[9,10] and low phosphor conversion efficiency for warm white LEDs.[11] GaN-based LEDs grown on sapphire substrates can achieve high efficiency, whereas sapphire substrates have low thermal conductivity, high insulating capability, and high costs for large-scale substrates. Hence, these imperfect characteristics hinder the development of LEDs for SSL. In recent years, GaN-on-Si LEDs have attracted a considerable amount of attention because they are inexpensive and highly suitable for large-scale manufacturing, indicating the potential of such LEDs in new types of SSL.[12] For the continued growth of GaN-on-Si, overcoming problems caused by a higher lattice mismatch and thermal expansion coefficient

*Address all correspondence to: Zen-Yu Li, E-mail: Chenyu.li@msa.hinet.net; Hao-Chung Kuo, E-mail: hckuo@faculty.nctu.edu.tw

1947-7988/2015/$25.00 © 2015 SPIE

Downloaded From: http://photonicsforenergy.spiedigitallibrary.org/ on 05/11/2015 Terms of Use: http://spiedl.org/terms

mismatch is essential. Low threading dislocation density (TDD) and crack-free large-scale GaN-on-Si LEDs are necessary for achieving high brightness and high efficiency.[13–16]

The asymmetric wurtzite structure of GaN and its strong built-in polarized field contribute to band bending in energy bands, which corresponds to the quantum confined Stark effect (QCSE) with poor internal quantum efficiency (IQE).[17] The strong electric field also causes severe electron leakage and poor hole injection in regions with multiple quantum wells (MQWs).[9] Hence, the IQE drops substantially when the driving current density increases, which is a reason for efficiency droop behavior.[9] Compared with GaN-based LEDs grown on sapphire substrates, GaN-on-Si LEDs have poor IQE because of the degraded crystal quality.

In order to minimize droop behavior, reducing carrier leakage and poor hole injection is crucial. However, related studies on improving droop behavior have focused on the design of barrier materials,[9,18] insertion layers between quantum wells (QWs) and quantum barriers (QBs),[19–21] electron blocking layers (EBLs),[13,22] modification of the GaN last barrier (LB) thickness,[23] and LED epitaxial layer growth on semipolar or nonpolar substrates.[8,24,25] Electric fields are sensitive to the thickness of QWs and QBs,[26,27] implying that modifying the thickness of QBs should improve droop behavior. Few previous studies have discussed improving the droop behavior by modifying the thickness of QBs,[28,29] and no study has considered this for GaN-on-Si LEDs. Therefore, we explored the improvement in efficiency droop behavior after modifying the thickness of QBs in GaN-on-Si LEDs. Furthermore, the growth of crack-free GaN-on-Si LEDs technology was investigated.

2 Experiments and Details

Epitaxial structures of GaN-on-Si LEDs were grown on 150-mm-diameter Si substrates by using a low-pressure metal-organic chemical vapor deposition system with a vertical reactor chamber (model: Veeco TurboDisc Maxbright C4). The liquid/solid precursors of trimethylgallium, trimethylindium, trimethylaluminum, and ammonia were used as the sources of the reactants Ga, In, Al, and N, respectively. Silane and bis-cyclopentadienyl-Mg were fabricated from the source of the *n*-type (Si) and *p*-type (Mg) dopants. The carrier gas was a mixture of gaseous N_2 and H_2. The substrates employed herein were 150-mm-diameter (111)-oriented Si substrates. The native oxide layers were removed before growth of the GaN materials. The wafer-cleaning procedures involved boiling the wafers in a 3∶1 ratio of $H_2SO_4:H_2O_2$ for 15 min and then dipping them in an hydrofluoric acid (HF) solution comprising HF and H_2O in a 1∶10 ratio for 15 s to remove the native oxide on the surface of the Si substrates. The Si substrate after loading was first heated to 1020 to 1050°C under ambient H_2 for 5 to 10 min to remove the surface-passivated layer. The underlayer structure was grown following the thermal cleaning procedure. The LED structure was grown on 150-mm-diameter Si(111) substrates with five levels of graded $Al_xGa_{1-x}N$ buffer layers (where x ranges from 0 to 1). Subsequently, 5-μm-thick crack-free undoped GaN with three AlN interlayers (ILs) was grown. The 2-nm-thick AlN ILs were inserted after 1.25-, 2.5-, and 3.75-μm-thick GaN epilayers were grown to suppress the TDD. Next, a 2.5-μm-thick *n*-type GaN (*n*-type doped $[\mathrm{Si}] = 1 \times 10^{19}\ \mathrm{cm}^{-3}$) layer was grown. The next 20 pairs of $In_{0.11}Ga_{0.89}N$/GaN (2 nm/2 nm) prestrained superlattices (SLs) were applied to improve the quality of the MQWs. Subsequently, 11 pairs of MQWs with 2-nm-thick $In_{0.22}Ga_{0.78}N$ QWs were grown. The thickness of the QBs was maintained at 13 nm for the first six pairs and modified for the last five pairs, among which two 13-nm-thick reference samples were reserved, and 10-, 8-, and 6-nm-thick QBs were introduced. The next 20-nm-thick InGaN LB was grown on MQWs and then the six pairs of $In_{0.02}Ga_{0.98}N/p\text{-}Al_{0.15}Ga_{0.85}N$ SLs EBL (SLs-EBL) were introduced (*p*-type doped $[\mathrm{Mg}] = 1 \times 10^{17}\ \mathrm{cm}^{-3}$). Subsequently, *p*-type GaN (*p*-type doped $[\mathrm{Mg}] = 5 \times 10^{18}\ \mathrm{cm}^{-3}$) was fabricated to complete the growth of the LED structure. Figure 1 shows a schematic diagram of the sample structures.

After the epitaxial growth, the LED chip was fabricated. An Si substrate exhibits strong absorption of visible light because of its small band gap of ∼1.12 eV. Hence, light with a wavelength of <1.1 μm is absorbed. Therefore, during the chip fabrication process of GaN-on-Si LEDs, the Si substrate should be removed. According to our previous research,[13] the GaN-on-Si LEDs were fabricated as a vertical chip with metal bonding on an Si template after the Si removal process was completed. The LED chip size was $1 \times 1\ \mathrm{mm}^2$, and the emission

Downloaded From: http://photonicsforenergy.spiedigitallibrary.org/ on 05/11/2015 Terms of Use: http://spiedl.org/terms

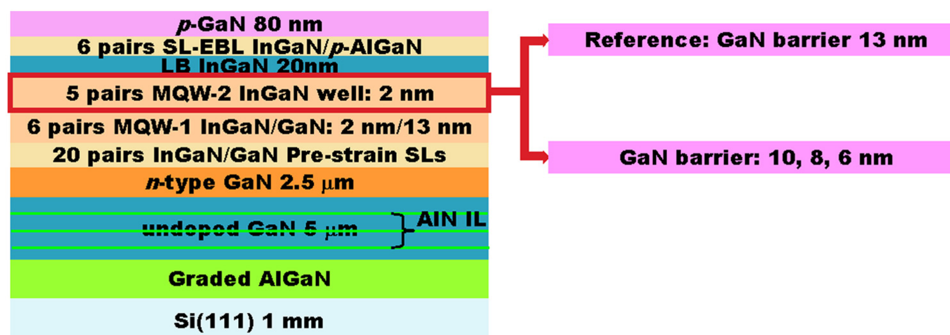

Fig. 1 Schematic diagram of the full GaN-on-Si light-emitting diode (LED) structure, reference structure design, and proposed structure design with thin barriers.

wavelengths were ~450 nm for all LEDs. Figure 2 shows a schematic diagram of the chip process flow and a top-view of the optical microscopy images of the chip.

The crystallinity of the epitaxial structures was evaluated using a high-resolution x-ray diffraction (HRXRD) microscope (model: Bede D1) with Cu K_α radiation as the x-ray source ($\lambda = 1.54056$ Å). The distribution of the threading dislocation in the epilayers was investigated using a high-resolution transmission electron microscope (model: JEOL 2100F) with a 0.1 nm lattice resolution. Temperature-dependent photoluminescence (TDPL) spectra were excited using a 325-nm He-Cd laser. The spectra were analyzed using a monochromator (model: Horiba Jobin Yvon *i*HR-550) and photomultiplier tubes. The electroluminescence spectra were measured at room temperature by using a probe station featuring a source meter in continuous-wave mode (model: Keithley 2400). Before device fabrication, the LEDs were first evaluated using simulation software (APSYS). The simulations were performed to determine the physical origin of the improved LED efficiency. The properties of the simulated structures, such as the layer thickness, doping concentration, and Al composition, were identical to the properties of the actual devices. Common physical parameters were adopted for the simulations, including a Shockley–Read–Hall recombination lifetime of 14 ns, and an Auger recombination coefficient in the QWs in the order of 9.5×10^{-32} $\mathrm{cm^6\,s^{-1}}$. The polarization-induced interface charge density was assumed to be a screening factor of 50%. The band-offset ratios were assumed to be 0.7:0.3 and 0.5:0.5 for InGaN and AlGaN, respectively.[30,31] Activation energy of the Mg dopant was defined as 170 meV for GaN; however, we assumed that the activation would be increased by 3 meV per Al% for AlGaN. Other material parameters used in the simulation can be found in Ref. 32.

3 Theorem and Calculations

Lin et al. initially explained and calculated the relationship between QB thickness and electric fields in MQWs.[28] Electric fields are affected by modifying QB thickness, possibly because the electric displacement field at the QW-QB interface is equal to a fixed charge density. The variables $\varepsilon_{\mathrm{QW}}$ and $\varepsilon_{\mathrm{QB}}$ denote the dielectric permittivity of the InGaN QW and GaN QB materials, respectively. The σ denotes the polarization charge density. The dielectric permittivity was calculated according to assumptions, with $\varepsilon_{\mathrm{QW}}$ and $\varepsilon_{\mathrm{QB}}$ set to $9.7\varepsilon_0$ and $8.9\varepsilon_0$, respectively. We obtained the electric fields in the MQWs as

$$E_{\mathrm{QB}} \approx -\frac{\sigma}{\varepsilon_{\mathrm{QW}}} \frac{1}{1 + (d_{\mathrm{QB}} + d_{\mathrm{QW}})} = -E_0 \frac{1}{1 + (d_{\mathrm{QB}}/d_{\mathrm{QW}})}, \tag{1}$$

$$E_{\mathrm{QW}} \approx -\frac{\sigma}{\varepsilon_{\mathrm{QW}}} \frac{1}{1 + (d_{\mathrm{QB}} + d_{\mathrm{QW}})} = +E_0 \frac{1}{1 + (d_{\mathrm{QW}}/d_{\mathrm{QB}})}, \tag{2}$$

where E_0 is defined as $\sigma/\varepsilon_{\mathrm{QW}}$. The polarization charge density σ was calculated to be 2.42×10^{-2} $\mathrm{C/m^2}$ at the interfaces of $\mathrm{In_{0.15}Ga_{0.85}N/GaN}$ MQWs, and E_0 was ~2.81 MV/cm.

Downloaded From: http://photonicsforenergy.spiedigitallibrary.org/ on 05/11/2015 Terms of Use: http://spiedl.org/terms

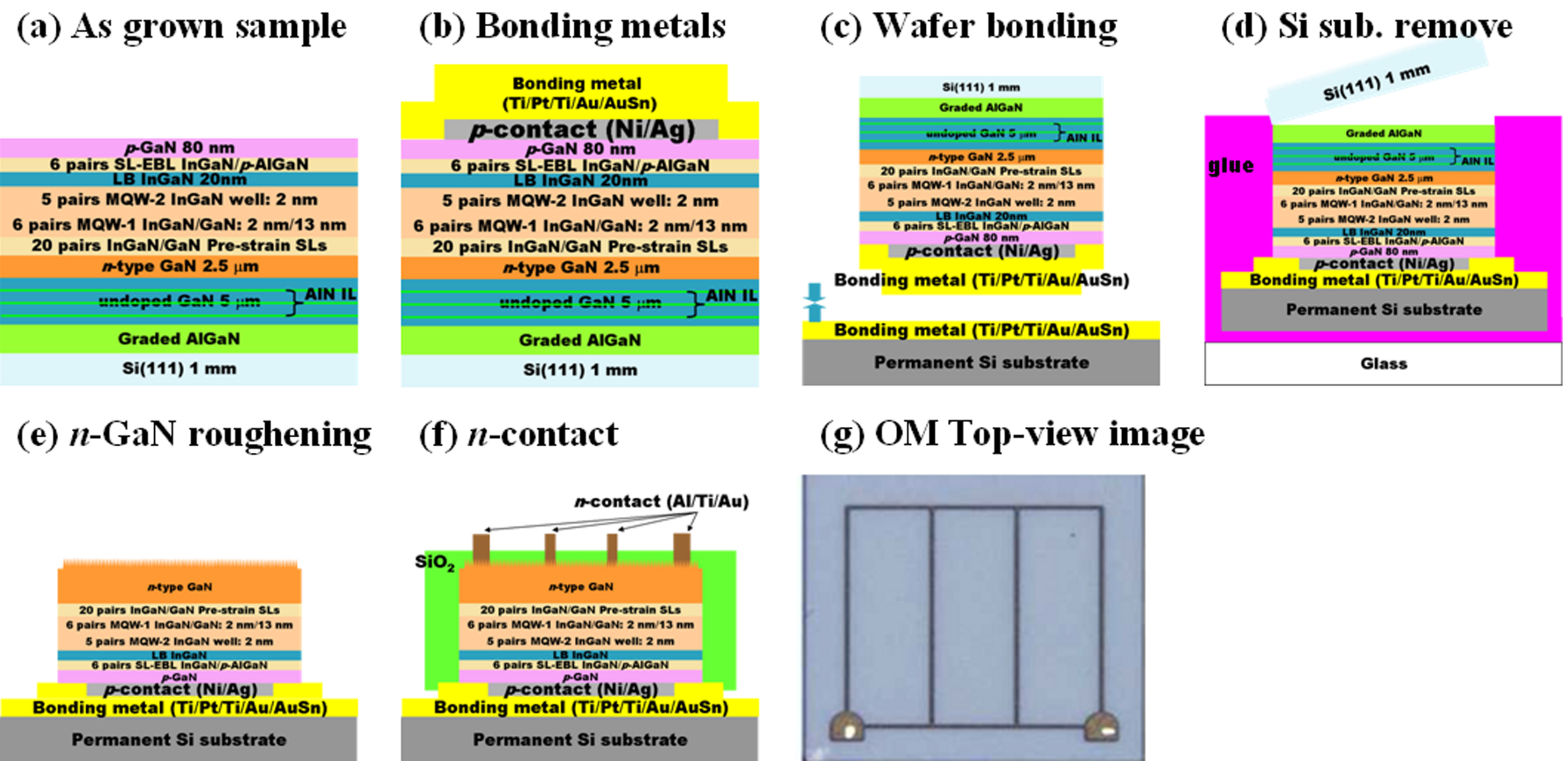

Fig. 2 Schematic diagrams of the vertical GaN-on-Si LED chip process flow: (a) as-grown GaN-on-Si LEDs, (b) deposition of *p*-metal layers and bonding metal layers when using an E-gun evaporator, (c) wafer bonding, (d) removal of the Si substrate by submerging it in an HNO_3:HF:$NaClO_2$ solution and then etching the buffer layers with inductivity coupled plasma reactive ion etching (ICP-RIE), (e) roughening of the *n*-GaN surface by submerging it in KOH, (f) deposition of the *n*-metal, which is then cut into 1×1 mm squares, (g) top-view optical microscopy image of the GaN-on-Si vertical chip.

Downloaded From: http://photonicsforenergy.spiedigitallibrary.org/ on 05/11/2015 Terms of Use: http://spiedl.org/terms

Equation (2) shows that the polarization-induced electric field was reduced by decreasing the QB thickness.[28]

To further analyze the electric field variation in the MQWs with the thin QBs, we simulated our LEDs structure as 13-, 10-, 8-, and 6-nm-thick GaN QBs composed of 2-nm-thick InGaN QWs. Varying the QB thickness was considered a suitable approach for studying the effect of QB thickness. Figure 3 shows the calculated electrostatic fields of LEDs at 700 mA; the positions of the five MQWs with modified QBs are marked in cyan. The figure shows that the reference LED exhibited a markedly stronger electrostatic field because of its high polarization-induced surface charge density. Stronger electrostatic fields in MQWs cause band bending, which refers to the separation of the electron and hole wave functions in the QWs and, hence, reduces the radiative recombination rate. The lower electric field was reduced by introducing the thinner QBs. Consequently, we obtained smaller negative electric fields of MQWs, which caused relaxed band bending in the MQWs and the elimination of the QCSE.

Figure 4 shows the band structure of the last MQW region with 6-, 8-, 10-, and 13-nm-thick QBs. In the figure, the band structure was shifted to align the left-hand interface between the GaN QB and InGaN QW; hence, we observed the slope variation of conduction band E_c in the QWs. Because the slopes of E_c were strongly dependent on the strength of the electric field in the QWs, the slopes became smaller when we reduced the thickness of the QBs. In the inset of Fig. 4, the enlarged scale of the band structures shows that the MQWs with thin QBs yielded smaller E_c slopes, which correspond with the simulated electric fields and are consistent with the calculated equations.

Figure 5 shows the variation of the E_c slopes under various current injections. The variable ΔE_c denotes the potential energy of the band offset in QWs. The lowest band offset was observed in the MQWs featuring the 6-nm-thick QBs, implying that the QCSE was improved by using this thickness. We anticipated a lower electroluminescence peak blueshift and expected the IQE to be further enhanced by reducing the thickness of the QBs. Table 1 summarizes the band offset in the MQWs during the various current injections in the MQWs with various QB thicknesses.

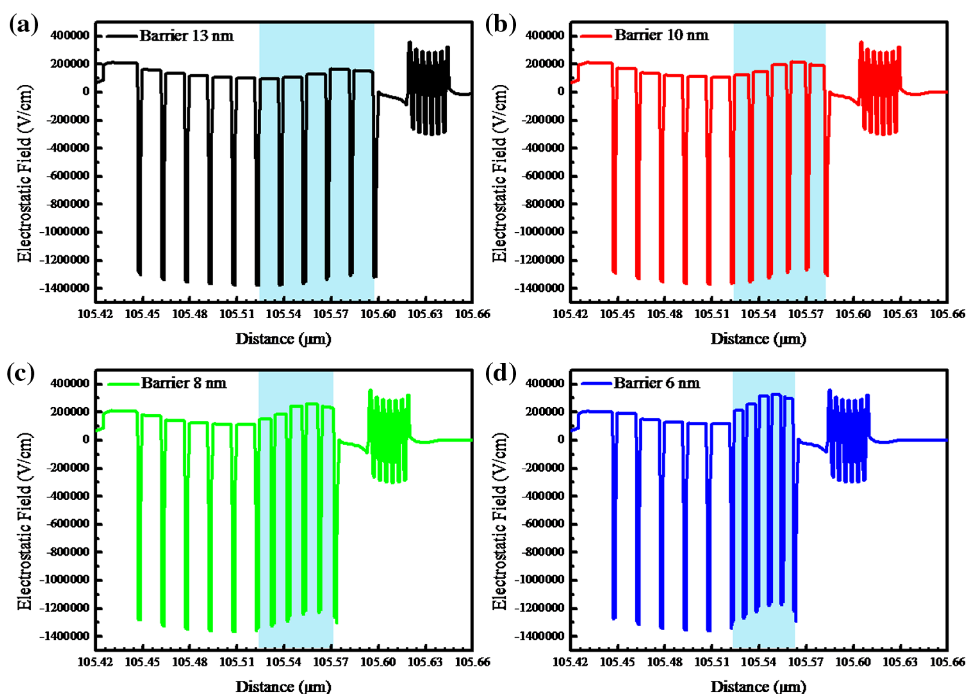

Fig. 3 Electrostatic fields of the multiple quantum wells (MQWs) and electron blocking layers (EBLs), which were measured at 700 mA: (a) reference 13-nm-thick quantum barriers (QBs), (b) 10-nm-thick QBs, (c) 8-nm-thick QBs, and (d) 6-nm-thick QBs.

Downloaded From: http://photonicsforenergy.spiedigitallibrary.org/ on 05/11/2015 Terms of Use: http://spiedl.org/terms

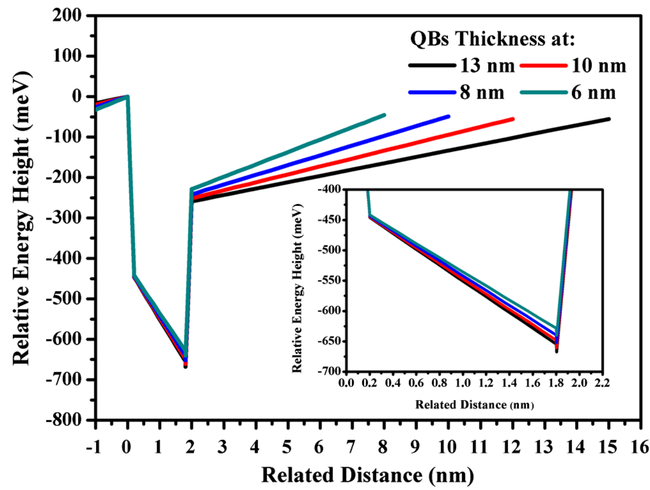

Fig. 4 Simulated energy band of an InGaN/GaN MQW structure with a 2-nm-thick QW and 13-nm-, 10-nm-, 8-nm-, and 6-nm-thick QBs. Energy band bending of the QWs is shown in the inset on an enlarged scale.

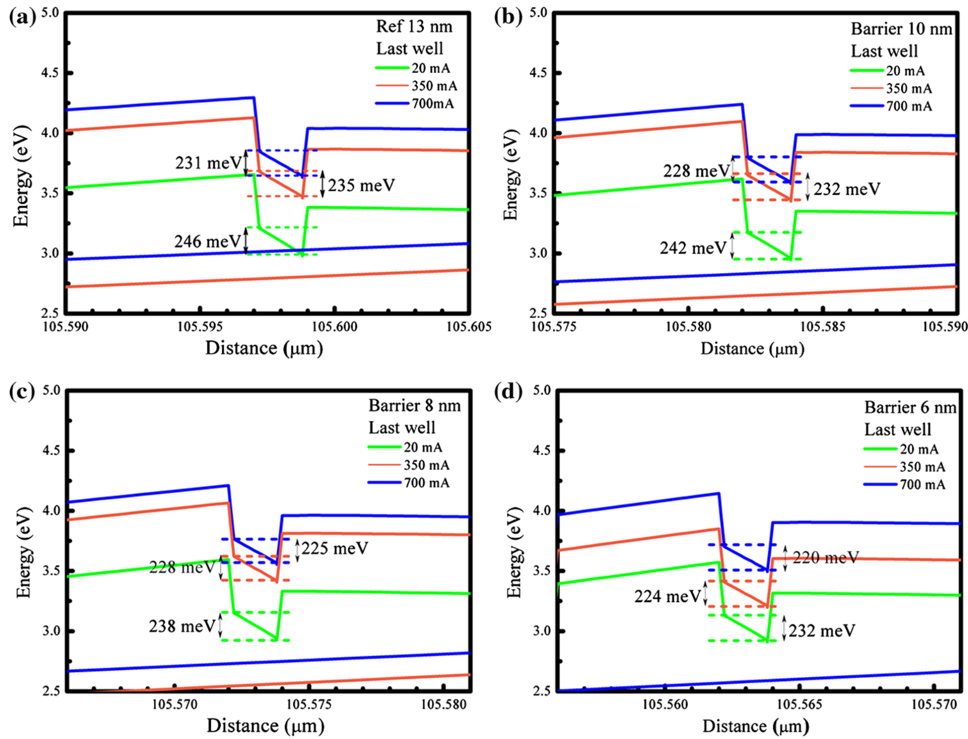

Fig. 5 Simulated band structure in the MQW structures with a 2-nm-thick QW and (a) 13-nm-thick QBs, (b) 10-nm-thick QBs, (c) 8-nm-thick QBs, and (d) 6-nm-thick QBs. The band offset of E_c is denoted as ΔE_c (marked on the band diagram).

Table 1 The band offset in quantum wells (QWs) with different current injected to multiple QWs.

Last well ΔE_c (meV)	Reference 13 nm	Barrier 10 nm	Barrier 8 nm	Barrier 6 nm
20 mA	246	242	238	232
350 mA	235	232	228	224
700 mA	231	228	225	220

Downloaded From: http://photonicsforenergy.spiedigitallibrary.org/ on 05/11/2015 Terms of Use: http://spiedl.org/terms

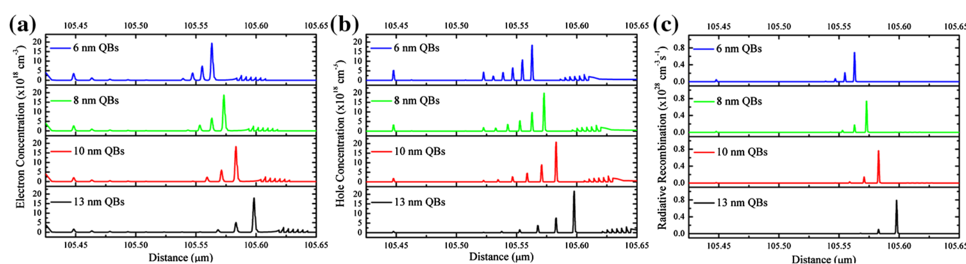

Fig. 6 (a) Electron concentration, (b) hole concentration, and (c) radiation recombination rate within the MQWs with various thicknesses of QBs at 700 mA.

The lower electric field with thin QBs in the MQWs also exhibited favorable carrier distribution and radiative recombination activities. Figures 6(a) and 6(b) show the calculated electron and hole distributions in the MQWs for the LEDs with various QB thicknesses at 700 mA.

The electron and hole distributions were improved in the MQWs. The favorable electron confinement was attributed to the lower electric field in the LB; hence, electron accumulation at the LB could be avoided to ensure that the distribution of electrons over the MQW was uniform.[33] Low electric fields also facilitated effective hole transport from the *p*-type GaN across the MQWs because the electric field-induced band bending was eliminated. Hence, the hole transport efficiency would be greatly improved.[22,28] However, a favorable distribution of carriers enhances the radiative recombination in the MQWs [Fig. 6(c)]. Furthermore, the lower negative electric field enhanced the QCSE; hence, the radiative recombination was strongly enhanced in the MQWs, particularly in the 6-nm-thick QBs.

Figure 7 shows the electron current density profiles near the MQWs of the LEDs corresponding to the various QB thicknesses at 700 mA. A drift-diffusion model was employed to calculate the electron current density and electron concentration. As shown in Fig. 7, the electron leakage could be eliminated by using the thin QBs. The reduced leakage was attributed to the favorable recombination observed in the MQWs featuring thin QBs. This result implies that reducing the thickness of the QBs can effectively eliminate electron leakage and enhance the radiative recombination.

The simulated band diagram and electrostatic field analysis show that the performance of the thin QBs was acceptable, indicating that the electric field was reduced by using thinner QBs. Figure 8 shows the simulated external quantum efficiency (EQE) versus the injection current of the LEDs for the 2-nm-thick QWs with 13-, 10-, 8-, and 6-nm-thick QBs. As the QB thickness decreased, a clear improvement in droop behavior was observed, with a reduction in droop

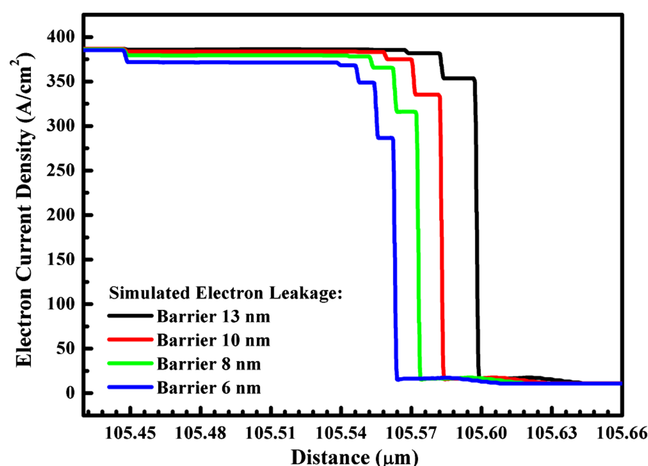

Fig. 7 Electron current density profiles near the MQWs for the LEDs with various thicknesses of QBs. The electron leakage was eliminated by reducing the QB thickness.

Downloaded From: http://photonicsforenergy.spiedigitallibrary.org/ on 05/11/2015 Terms of Use: http://spiedl.org/terms

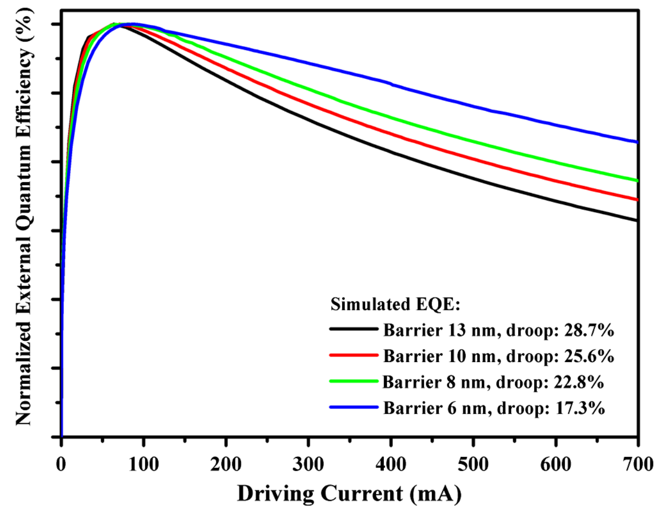

Fig. 8 Simulated external quantum efficiency (EQE) for the GaN-on-Si LEDs with various QB thicknesses.

behavior efficiency from 28.7% in the 13-nm-thick reference LED to 17.3% in the 6-nm-thick thin QB LEDs. This result indicates that reducing the thickness of the QBs improved the performance in droop behavior. The marked improvement in the droop behavior efficiency can mainly be attributed to enhancing the hole injection and electron confinement, particularly at high injection currents. Therefore, raising the droop-onset current should generate a higher peak EQE.[34]

4 Results and Discussion

4.1 *Structural Analysis*

First, cracking and circular defects were clearly observable on the surface of GaN-on-Si because of the substantial thermal expansion coefficient mismatch and the reaction of Ga and Si atoms out-diffusing from the substrate.[35] The large difference in thermal expansion coefficients between the GaN ($5.59 \times 10^{-6}\ K^{-1}$) and Si ($2.59 \times 10^{-6}\ K^{-1}$) produced tensile stress in GaN and caused cracking during cooling after epitaxial growth. In this study, no cracking or Ga melt-back etching was observed on the 150-mm-diameter GaN-on-Si LEDs, indicating that the epitaxy was effectively controlled. The HRXRD rocking curves of the GaN-on-Si LEDs (Fig. 9) show the crystal qualities of the (0002) plane and ($10\bar{1}2$) plane, respectively. The full width at half maximum (FWHM) of the (0002) peak was ~347.0 arcsec but shows 473.9 arcsec

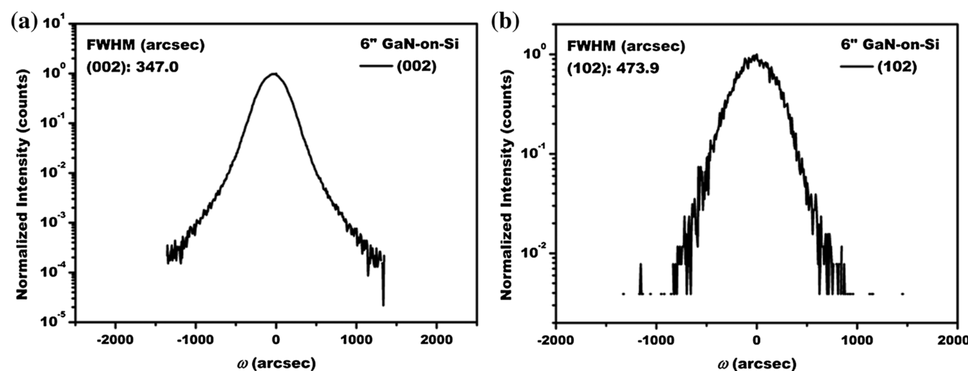

Fig. 9 High-resolution x-ray diffraction rocking curves for the (a) (0002) and (b) ($10\bar{1}2$) planes of the GaN-on-Si LEDs.

Downloaded From: http://photonicsforenergy.spiedigitallibrary.org/ on 05/11/2015 Terms of Use: http://spiedl.org/terms

for the $(10\bar{1}2)$ plane, respectively. The FWHM of the peaks might contribute to the crystal quality and be related to the TDD. In wurtzite crystal structures of GaN, screw-type or mixed-type dislocation densities are related to the FWHM of the (0002) peak in the XRD rocking curve; furthermore, the total dislocations' density is related to the FWHM of the $(10\bar{1}2)$ peak in the XRD rocking curve.[36] The dislocation densities in various types of structures can be roughly calculated using an equation.[37] In this study, we estimated the total dislocation density to be $\sim 7 \times 10^8\ \mathrm{cm}^{-2}$, which is in close agreement with the results from our previous study involving a similar epitaxial structure.[13]

TEM images were obtained to analyze the crystal structure and epitaxial quality of the GaN-on-Si LEDs. Figure 10(a) shows a scanning TEM (STEM) image of the GaN-on-Si LEDs with a zone axis where $\vec{g} = [11\bar{2}0]$. The five levels of graded $Al_xGa_{1-x}N$ buffer layers and undoped GaN with three AlN ILs were clearly observed. The threading dislocations (TDs) were gradually reduced from the undoped GaN underlayer or the active layers when the three AlN ILs were introduced. Figure 10(b) shows the STEM high-angle annular dark field (STEM-HAADF) image of the SLs-EBL, MQWs, and prestrained SLs. The last five pairs of the MQWs with the 8-nm-thick QBs are clearly observable in the figure. Furthermore, the clear interface of the MQWs is visible in the STEM bright-field image in Fig. 10(c), indicating that favorable strain management in the MQWs was observed when the 20 pairs of prestrained SLs were introduced.

To verify the crystalline quality of the GaN-on-Si LEDs, we observed and calculated the TDD by using TEM two-beam condition imaging. Heying et al. indicated that pure edge-type and mixed-type TDD can be identified under the two-beam condition with a zone axis where $\vec{g} = [1\bar{1}00]$, whereas pure screw-type and mixed-type TDD can be identified under the two-beam condition with a zone axis where $\vec{g} = [0002]$.[36] Figures 11(a)–11(c) are TEM images of the first undoped GaN underlayer grown on an Si substrate. Figure 11(a) is the original image with a zone axis where $\vec{g} = [11\bar{2}0]$, with Figs. 11(b) and 11(c) showing the TEM two-beam condition image with a zone axis where $\vec{g} = [0002]$ and $\vec{g} = [1\bar{1}00]$, respectively. In this series of images, few screw-type TDs were observed, whereas many TDs were observed at the interface between the graded $Al_xGa_{1-x}N$ buffer layers and the Si substrate. The total TDD, including edge-type, screw-type, and mixed-type TDs, was estimated to exceed $10^{10}\ \mathrm{cm}^{-2}$ at the interface between the graded $Al_xGa_{1-x}N$ buffer layers and the Si substrate, and the TDD gradually decreased to $\sim 10^9\ \mathrm{cm}^{-2}$ in the first undoped GaN region. Figures 11(d)–11(f) are TEM images of the undoped GaN underlayer grown on Si with AlN ILs. The TDs remained observable in the GaN layer, but the TDD was markedly reduced after introducing the three ILs. The densities of the edge-type, mixed-type, and screw-type TDs were estimated to be 5.3×10^8, 1.0×10^9, and $<1 \times 10^7\ \mathrm{cm}^{-2}$, respectively. The total TDD in the uppermost layer of the undoped GaN region was further reduced to $\sim 8.0 \times 10^8\ \mathrm{cm}^{-2}$, corresponding to the HRXRD results and yielding a total TDD of ~ 7 to $8 \times 10^8\ \mathrm{cm}^{-2}$. Hence, the total TDD in the region of active layers was reasonably estimated at $<7 \times 10^8\ \mathrm{cm}^{-2}$.

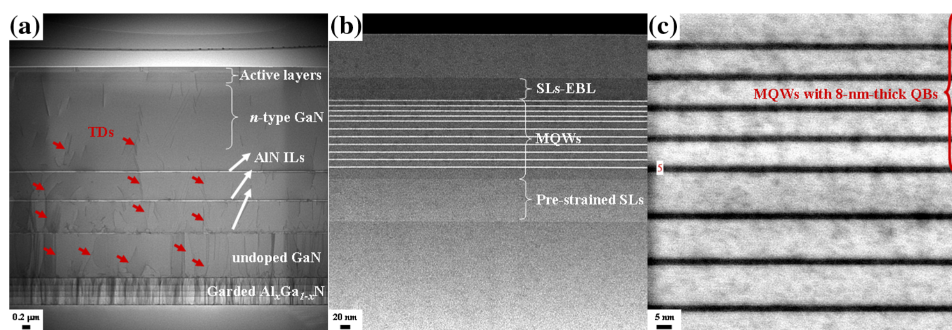

Fig. 10 (a) Scanning transmission electron microscope (STEM) image of the entire GaN-on-Si LED structure. (b) STEM-HAADF image of the prestrained superlattices (SLs), MQWs, and SL EBL. (c) STEM image of the MQWs with $\bar{g} = [1\bar{1}00]$. The interface and 8-nm-thick QBs are clearly visible.

Downloaded From: http://photonicsforenergy.spiedigitallibrary.org/ on 05/11/2015 Terms of Use: http://spiedl.org/terms

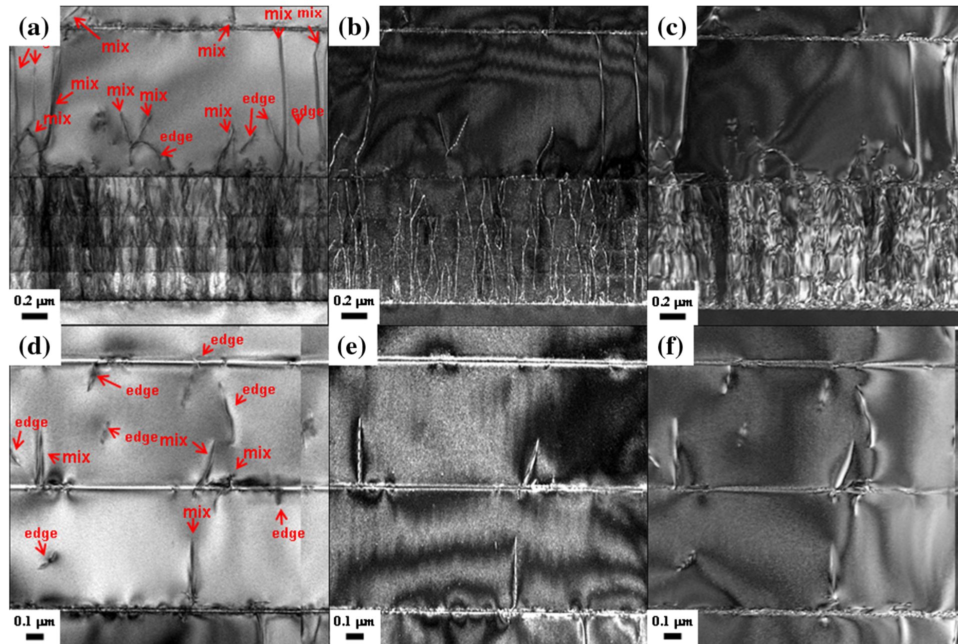

Fig. 11 (a) to (c) TEM images of the first undoped GaN underlayer grown on Si. (a) is the original image with a zone axis where $\vec{g} = [11\bar{2}0]$. (b) and (c) show the TEM two-beam condition with a zone axis where $\vec{g} = [0002]$ and $\vec{g} = [1\bar{1}00]$, respectively. (d) to (f) TEM images of the undoped GaN underlayer grown on Si with AlN interlayers. (d) is the original image with a zone axis where $\vec{g} = [11\bar{2}0]$. (e) and (f) show the TEM two-beam condition with a zone axis where $\vec{g} = [0002]$ and $\vec{g} = [1\bar{1}00]$, respectively.

4.2 *Device Analysis*

Figure 12 shows the measured EQE versus driving current. The droop behaviors in the simulated EQE curves corresponded with the experimental data. Moreover, the peak EQE was gradually reduced from the thicker QBs to the thinner QBs. The LED featuring the 6-nm-thick QBs exhibited the smallest droop behavior, but yielded a poor peak EQE (46.13%). Compared with the simulated EQE (Fig. 8), the lowest droop behavior was observed in the LED featuring the 6-nm-thick QBs; however, the light output power (LOP) was not considered. By contrast, the LOP clearly decreases, as shown in the experimental curve of the LEDs with the 6-nm-thick QBs.

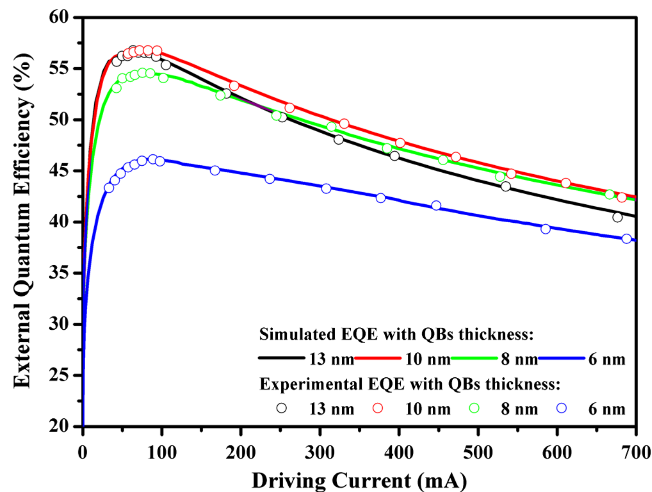

Fig. 12 Comparison of the EQEs of the LEDs. The EQEs were observed in the conventional QBs with a thickness of 13, 10, 8, and 6 nm. The simulated EQE curves are represented by the solid lines and the experimental results are marked by the circles.

Downloaded From: http://photonicsforenergy.spiedigitallibrary.org/ on 05/11/2015 Terms of Use: http://spiedl.org/terms

This unexpected phenomenon can be attributed to the lower crystal quality and the lower thermal treatment of the QWs. Previous studies have shown that decorating the size and distribution of InGaN quasiregular quantum dots (QDs) is necessary during the thermal treatment involved in growing QBs. The thermal treatment of InGaN QDs may be crucial for achieving high brightness and acceptable EQE performance.[38,39] Furthermore, Kim et al. reported that the FWHMs of x-ray rocking curves of InGaN/GaN MQWs with GaN QB thicknesses of 5.6, 16.7, and 22.4 nm were broader than those of InGaN/GaN MQWs with a GaN QB thickness of 10.4 nm,[40] indicating that the crystal quality of exceedingly thin QBs is degraded and would further reduce the LOP. To further investigate the density of QDs, we calculated the activation energy of the localized state through TDPL, which is a method reported in Ref. 41. The integrated PL intensities were plotted as a function of temperature, which can be expressed as the Arrhenius equation:

$$I_{\mathrm{PL}}(T) = \frac{I_0}{1 + Ae^{(-E_\mathrm{a}/k_\mathrm{B}T)}}, \tag{3}$$

where A is a constant, E_a denotes the activation energy, and k_B is Boltzmann's constant. An increase in activation energy indicates strong carrier localization in In clustering regions. The origin of the localization center can be ascribed to a self-formed In-rich region that might act as an InGaN QD.[42] The emission intensity increases in the presence of a stronger quantum confinement effect in InGaN QDs.[43] In the present study, we also plotted the TDPL and integrated PL intensities as a function of temperature (Fig. 13).

The activation energies of radiative recombination peaks are also plotted in Fig. 13, in which the activation energies of the 13-, 10-, 8-, and 6-nm-thick QBs are 43.5, 42.8, 39.6, and 31.4 meV, respectively. This result is in close agreement with the strong carrier localizations in the 13-nm-thick QBs, indicating that a higher density of QDs was obtained in the 13-nm-thick QBs, whereas a lower density of QDs was obtained in the 6-nm-thick QBs. Therefore, the thin barrier implies that less thermal treatment is required for the QDs and the LOP decreases with a lower peak EQE. Although the droop behavior was improved by introducing the 6-nm-thick QBs, a drop in EQE occurred, rendering the 6-nm-thick QBs unsuitable for use in LEDs. In addition, we observed that the LED with 8-nm-thick QBs exhibited acceptable droop behavior (from 28.5% in the reference to 22.9% in the 8-nm-thick sample); however, the peak EQE was not markedly reduced, peaking at 54.6%. This result implies that the LEDs with thin QBs achieved acceptable performance according to the EQE curve; thus, the optimal thickness of QBs was 8 nm.

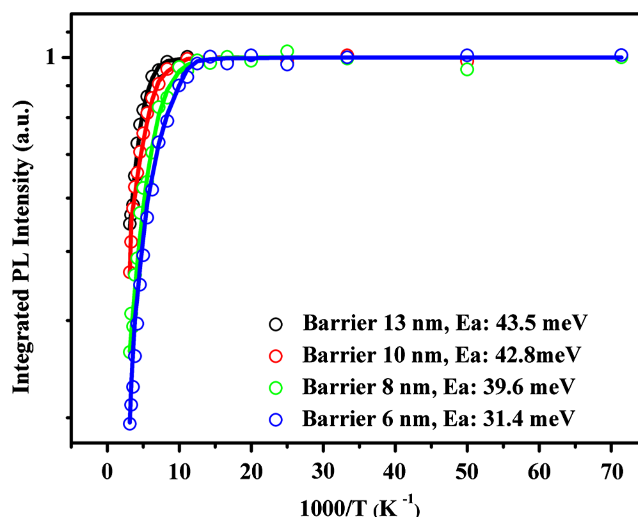

Fig. 13 Plot of the integrated emission intensity as a function of temperature, which was measured using conventional 13-, 10-, 8-, and 6-nm-thick QBs.

Downloaded From: http://photonicsforenergy.spiedigitallibrary.org/ on 05/11/2015 Terms of Use: http://spiedl.org/terms

5 Conclusion

Crack-free 150-mm-diameter GaN-on-Si LEDs with improved droop behavior were achieved. The strain management properties of the graded $Al_xGa_{1-x}N$ buffer layer caused the crack-free GaN-on-Si LED surface. In addition, the TDD of GaN-on-Si LEDs was reduced to $<7 \times 10^8\ \mathrm{cm}^{-2}$, providing a suitable platform for achieving an acceptable LED performance. The simulated results indicate that the thin QBs produced acceptable droop behavior because the polarization-induced electrostatic field was eliminated. Furthermore, hole injection and electron leakages were improved. Therefore, the lowest droop behavior, which was reduced from 28.7% to 17.3%, was observed in the LEDs featuring 6-nm-thick QBs. However, the experimental results revealed an unanticipated phenomenon. Through the thinner design of QBs, the droop behavior of the LEDs with the 6-nm-thick QBs was only 17.7%, but the worst peak EQE was only 46.13%. Hence, the LEDs featuring the 8-nm-thick QBs exhibited acceptable droop behavior (22.9%) and peak EQE (54.6%). In summary, we recommend using LEDs featuring 8-nm-thick QBs to improve droop behavior.

Acknowledgments

This work was funded by the National Science Council in Taiwan under Grant Number MOST 103-3113-E-009-001-CC2. We thank Professor Chien-Chung Lin from College of Photonics, National Chiao Tung University, and Professor Ray-Ming Lin from Department of Electronic Engineering, Chang Gung University, for the instruction of the light-emitting diode analysis. We also acknowledge Epistar Inc. for supporting samples to this work.

References

1. S. Nakamura et al., "InGaN based multi-quantum-well-structure laser diodes," *Jpn. J. Appl. Phys.* **35**(Part 2, No. 1B), L74–L76 (1996).
2. H. P. Zhao et al., "Approaches for high internal quantum efficiency green InGaN light-emitting diodes with large overlap quantum wells," *Opt. Express* **19**(S4), A991–A1007 (2011).
3. M. R. Krames et al., "Status and future of high-power light-emitting diodes for solid-state lighting," *J. Disp. Technol.* **3**(2), 160–175 (2007).
4. M. H. Crawford, "LEDs for solid-state lighting: performance challenges and recent advances," *IEEE J. Sel. Topics Quantum Electron.* **15**(4), 1028–1040 (2009).
5. N. G. Young et al., "High performance thin quantum barrier InGaN/GaN solar cells on sapphire and bulk (0001) GaN substrates," *Appl. Phys. Lett.* **103**, 173903 (2013).
6. B. N. Pantha et al., "Erbium-doped AlInGaN alloys as high-temperature thermoelectric materials," *Appl. Phys. Express* **4**(5), 051001 (2011).
7. J. Zhang et al., "High-temperature characteristics of Seebeck coefficients for AlInN alloys grown by metalorganic vapor phase epitaxy," *J. Appl. Phys.* **110**(4), 043710 (2011).
8. H. Sato et al., "Optical properties of yellow light-emitting diodes grown on semipolar (11 2) bulk GaN substrates," *Appl. Phys. Lett.* **92**, 221110 (2008).
9. M. H. Kim et al., "Origin of efficiency droop in GaN-based light-emitting diodes," *Appl. Phys. Lett.* **91**, 183507 (2007).
10. J. Piprek, "Efficiency droop in nitride-based light-emitting diodes," *Phys. Stat. Sol. A, Appl. Mater. Sci.* **207**(10), 2217–2225 (2010).
11. S. P. Chang et al., "Electrically driven green, olivine, and amber color nanopyramid light emitting diodes," *Opt. Express* **21**, 23030–23035 (2013).
12. S. Nakamura, T. Mukai, and M. Senoh, "Candela-class high-brightness InGaN/AlGaN double-heterostructure blue-light-emitting diodes," *Appl. Phys. Lett.* **64**(13), 1687–1689 (1994).
13. Z. Y. Li et al., "High-efficiency and crack-free InGaN-based LEDs on a 6-inch Si (111) substrate with a composite buffer layer structure and quaternary superlattices electron-blocking layers," *IEEE J. Quantum Electron.* **50**(5), 354–363 (2014).
14. R. H. Horng et al., "Performance of GaN-based light-emitting diodes fabricated using GaN epilayers grown on silicon substrates," *Opt. Express* **22**(S1), A179–A187 (2014).
15. C. Y. Cho et al., "Surface plasmon enhanced light emission from AlGaN-based ultraviolet light-emitting diodes grown on Si (111)," *Appl. Phys. Lett.* **102**(21), 211110 (2013).

Downloaded From: http://photonicsforenergy.spiedigitallibrary.org/ on 05/11/2015 Terms of Use: http://spiedl.org/terms

16. H. Song et al., "Effects of enhanced lateral transport on InGaN/GaN light emitting diodes via n-type AlGaN/GaN superlattices," *Appl. Phys. Lett.* **103**(14), 141102 (2013).
17. M. F. Schubert and E. F. Schubert, "Effect of heterointerface polarization charges and well width upon capture and dwell time for electrons and holes above GaInN/GaN quantum wells," *Appl. Phys. Lett.* **96**(13), 131102 (2010).
18. H. Zhao et al., "Analysis of internal quantum efficiency and current injection efficiency in III-nitride light-emitting diodes," *J. Disp. Technol.* **9**(4), 212–225 (2013).
19. N. Tansu et al., "III-nitride photonics," *IEEE J. Photonics* **2**(2), 241–248 (2010).
20. H. Zhao et al., "Current injection efficiency induced efficiency-droop in InGaN quantum well light-emitting diodes," *Solid-State Electron.* **54**(10), 1119–1124 (2010).
21. G. Liu et al., "Efficiency-droop suppression by using large-bandgap AlGaInN thin barrier layers in InGaN quantum-well light-emitting diodes," *IEEE J. Photonics* **5**(2), 2201011 (2013).
22. B. C. Lin et al., "Hole injection and electron overflow improvement in InGaN/GaN light-emitting diodes by a tapered AlGaN electron blocking layer," *Opt. Express* **22**, 463–469 (2014).
23. S. H. Yen et al., "Investigation of optical performance of InGaN MQW LED with thin last barrier," *IEEE Photon. Technol. Lett.* **22**(24), 1787–1789 (2010).
24. C. H. Chiu et al., "Reduction of efficiency droop in semipolar (1101) InGaN/GaN light emitting diodes grown on patterned silicon substrates," *Appl. Phys. Express* **4**(1), 012105 (2011).
25. Y. Zhao et al., "High-power blue violet semipolar (2021) InGaN/GaN light-emitting diodes with low efficiency droop at 200 A/cm^2," *Appl. Phys. Express* **4**(8), 082104 (2011).
26. C. K. Wang et al., "Investigating the effect of piezoelectric polarization on GaN-based LEDs with different quantum barrier thickness," *IEEE J. Disp. Technol.* **9**(4), 206–211 (2013).
27. M. Leroux et al., "Barrier-width dependence of group-III nitrides quantum-well transition energies," *Phys. Rev. B* **60**(3), 1496–1499 (1999).
28. G. B. Lin et al., "Effect of quantum barrier thickness in the multiple-quantum-well active region of GaInN/GaN light-emitting diodes," *IEEE J. Photonics* **5**(4), 1600207 (2013).
29. B. C. Chen et al., "Improved performance of InGaN/GaN light-emitting diodes with thin intermediate barriers," *IEEE Photon. Technol. Lett.* **23**(22), 1682 (2011).
30. J. Piprek and S. Nakamura, "Physics of high-power InGaN/GaN lasers," *IEE Proc. Optoelectron.* **149**, 145 (2002).
31. J. Piprek, "Ultra-violet light-emitting diodes with quasi acceptor-free AlGaN polarization doping," *Opt. Quantum Electron.* **44**(3), 67–73 (2012).
32. I. Vurgaftman and J. R. Meyer, "Band parameters for nitrogen-containing semiconductors," *J. Appl. Phys.* **94**(6), 3675–3696 (2003).
33. V. Avrutin et al., "InGaN light-emitting diodes: efficiency-limiting processes at high injection," *J. Vac. Sci. Technol. A* **31**, 050809 (2013).
34. G. B. Lin et al., "Analytic model for the efficiency droop in semiconductors with asymmetric carrier-transport properties based on drift-induced reduction of injection efficiency," *Appl. Phys. Lett.* **100**(16), 161106 (2012).
35. M. Wei et al., "Effect of AlN buffer thickness on GaN epilayer grown on Si(1 1 1)," *Mater. Sci. Semicond. Process.* **14**(2), 97–100 (2011).
36. B. Heying et al., "Role of threading dislocation structure on the x-ray diffraction peak widths in epitaxial GaN films," *Appl. Phys. Lett.* **68**(5), 643–645 (1996).
37. S. R. Lee et al., "Effect of threading dislocations on the Bragg peakwidths of GaN, AlGaN, and AlN heterolayers," *Appl. Phys. Lett.* **86**(24), 241904 (2005).
38. Y. S. Lin et al., "Quasiregular quantum-dot-like structure formation with postgrowth thermal annealing of InGaN/GaN quantum wells," *Appl. Phys. Lett.* **80**(14), 2571–2573 (2002).
39. Z. Y. Li et al., "Carrier localization degree of $In_{0.2}Ga_{0.8}N/GaN$ multiple quantum wells grown on vicinal sapphire substrates," *J. Appl. Phys.* **105**, 013103 (2009).
40. D. J. Kim et al., "Effect of barrier thickness on the interface and optical properties of InGaN/GaN multiple quantum wells," *Jpn. J. Appl. Phys.* **40**, 3085–3088 (2001).
41. H. K. Cho et al., "Influence of strain-induced indium clustering on characteristics of InGaNÕGaN multiple quantum wells with high indium composition," *J. Appl. Phys.* **91**(3), 1104–1107 (2002).
42. Y. Narukawa et al., "Recombination dynamics of localized excitons in $In_{0.20}Ga_{0.80}N$-$In_{0.05}Ga_{0.95}N$ multiple quantum wells," *Phys. Rev. B* **55**(4), R1398–R1941 (1997).

Downloaded From: http://photonicsforenergy.spiedigitallibrary.org/ on 05/11/2015 Terms of Use: http://spiedl.org/terms

43. C. C. Chuo et al., "Effects of thermal annealing on the luminescence and structural properties of high indium-content InGaN/GaN quantum wells," *Appl. Phys. Lett.* **76**(26), 3902–3904 (2000).

An-Jye Tzou received his BS and MS degrees in electronic engineering from Chung Yuan Christian University, Chungli, Taiwan, in 2008 and 2010, respectively. He is currently pursuing the PhD degree with the Department of Electrophysics, NCTU. He joined the Semiconductor Laser Technology Laboratory, NCTU, in July 2012. His current research interests include III-V compound semiconductor materials growth by MOCVD.

Bing-Cheng Lin received his BS degree in electrical engineering from Feng Chia University, Taichung, Taiwan, in 2002, and his MS degree in the Institute of Photonics Physics from National Changhua University of Education (NCUE), Taiwan, in 2011. He is currently working toward the PhD degree in the Department of Photonics and the Institute of Electron-Optical Engineering, NCTU. His current research interests in III-nitride optoelectronic devices simulations.

Chia-Yu Lee received his BS degree in electrical engineering from Feng Chia University, Taichung, Taiwan, and his MS degree in optical sciences from National Central University, Zhongli, Taiwan, in 2005 and 2009, respectively. He is currently pursuing the PhD degree in the Institute of Electro-Optical Engineering, National Chiao Tung University, Hsinchu, Taiwan. His current research interests include III–V compound semiconductor materials growth on silicon substrates.

Da-Wei Lin received his BS and MS degrees in photonics from National Chiao Tung University, Hsinchu, Taiwan, in 2009 and 2010, respectively, where he is currently pursuing the PhD degree in photonics. His current research interests include the epitaxy of III–V compound semiconductor materials by MOCVD and analysis for GaN-based light-emitting diodes.

Yu-Kuang Liao received his BS degree in physics from National Chung Cheng University (NCCU), Taiwan, in 2008. He received his MS degree in electrophysics from NCTU and his PhD degree in Semi-conductor Laser Laboratory in 2014. His current research interests are in optoelectronic device fabrication and characterization, such as hybrid nano-crystal quantum dots solar cells, thin film Cu(In,Ga)Se2 solar cells, and wide-bandgap materials.

Zhen-Yu Li received his BS degree in electronic engineering from Chung Yuan Christian University, Taiwan, in 2003, and his PhD degree in engineering from Chung Yuan Christian University, Taiwan, in 2007. He is a senior postdoctoral research fellow in Academia Sinica (2014 to current). His current research interests are in wide bandgap materials and devices.

Gou-Chung Chi received his BS degree from the National Taiwan Normal University, Taiwan, in 1970, and his MS and PhD degrees in solid state physics and materials, Department of Engineering and Applied Science from Yale University, in 1973 and 1976, respectively. Since 2009, he is a professor of the Department of Photonics, NCTU. His recent research interests are wide band gap semiconductor and devices.

Hao-Chung Kuo received his BS degree in physics from National Taiwan University, Taiwan, his MS degree in electrical and computer engineering from Rutgers University, New Brunswick, New Jersey, in 1995, and his PhD degree from the Electrical and Computer Engineering Department, University of Illinois at Urbana Champaign, in 1999. He is now the professor, Department of Photonics and Institute of Electro-Optical Engineering, NCTU. His current research interests include VCSELs, blue and UV LED, and solar cells.

Chun-Yen Chang received his BS degree in electrical engineering from the National Cheng Kung University (NCKU), Tainan, Taiwan, in 1960 and his MS and PhD degrees from the National Chiao Tung University (NCTU), Hsinchu, Taiwan, in 1962 and 1969, respectively. He was the president of NCTU, and a fellow of Academia Sinica, IEEE life Fellow, and is regarded as "the father of Taiwan semiconductor industries."

Downloaded From: http://photonicsforenergy.spiedigitallibrary.org/ on 05/11/2015 Terms of Use: http://spiedl.org/terms